SAN099-2411J

Equivalent-Circuit Model for the Thickness-Shear Mode Resonator with a Viscoelastic Film near Film Resonance

Stephen J. Martin,* Helen L. Bandey, and Richard W. Cernosek

Microsensor Research and Development Department, Sandia National Laboratories, Albuquerque, New Mexico 87185-1425

A. Robert Hillman and Mark J. Brown

Chemistry Department, Leicester University, Leicester, LE1 7RH, U.K.

ABSTRACT

We derive a lumped-element, equivalent-circuit model for the thickness shear mode (TSM) resonator with a viscoelastic film. This modified Butterworth-Van Dyke model includes in the motional branch a series LCR resonator, representing the quartz resonance, and a parallel LCR resonator, representing the film resonance. This model is valid in the vicinity of film resonance, which occurs when the acoustic phase shift across the film is an odd multiple of $\pi/2$ radians. This model predicts accurately the frequency changes and damping that arise at resonance and is a reasonable approximation away from resonance. The elements of the model are explicitly related to film properties and can be interpreted in terms of elastic energy storage and viscous power dissipation. The model leads to a simple graphical interpretation of the coupling between the quartz and film resonances and facilitates understanding of the resulting responses. These responses are compared with predictions from the transmission-line and the Sauerbrey models.

KEYWORDS

Thickness-shear mode resonator; quartz crystal microbalance; viscoelasticity; film resonance; equivalent circuit; lumped-element model; transmission-line model.

* To whom correspondence should be addressed.

DISCLAIMER

DISCLAIMER

Portions of this document may be illegible in electronic image products. Images are produced from the best available original document.

INTRODUCTION

The thickness-shear mode (TSM) resonator consists of a thin disk of AT-cut quartz with metal electrodes deposited on both sides (Fig. 1a). Mechanical vibrations are excited in the piezoelectric quartz when an alternating potential is applied to the electrodes. Predominantly shear modes are excited in the AT-cut of quartz, with displacement parallel to the quartz surfaces (Fig. 1b). Resonances are excited at frequencies for which the quartz thickness corresponds to an odd multiple of half the acoustic wavelength.

When a film is deposited on the quartz resonator (Fig. 2), the oscillating surface interacts mechanically with the layer.[1,2] Due to the piezoelectric properties of the quartz, this mechanical interaction is reflected in the electrical properties of the quartz.[1] Thus, electrical measurements on the resonator can be used to extract mechanical properties of the layer.[1-6]

The transmission-line model shown in Fig. 3 describes the electrical response of the quartz resonator with a film. The quartz resonator is represented by the Mason model[7] (lower portion), in which the transmission line (from plane EF to plane IJ) represents acoustic propagation across the quartz; this acoustic signal is coupled to the electrical port (AB) via a transformer (the turns ratio n is proportional to the quartz electromechanical coupling factor, K^2). In the transmission line, voltage represents shear stress, while current represents shear particle velocity. When the quartz resonator is uncoated, both surfaces are stress free—represented by a short-circuit termination at ports IJ and EF. In this case, the Mason model predicts a very sharp enhancement in admittance (ratio of current flow to applied voltage) at the quartz resonant frequencies; this can be traced to constructive interference between the waves launched electrically (at port CD) and those reflected back by the stress-free quartz surfaces. A viscoelastic film coating the device surface is represented by a lossy transmission line (EF-GH) coupled to an acoustic port of the Mason model. Since the upper surface of the film is stress-free, acoustic port GH is terminated in a short.

The effect of a film on the resonator response depends on the mechanical impedance (ratio of stress to particle velocity) contributed by the layer; this depends on the acoustic properties of the layer as well as *interference* between the waves reflected by the two film surfaces. This interference depends on the phase shift and attenuation experienced by the acoustic wave in propagating across the film.

If the film coating the TSM resonator is sufficiently thin and rigid that the displacement imposed at the quartz/film interface propagates across with negligible phase shift (i.e., the layer is "acoustically thin"), then the layer moves synchronously with the resonator surface. In this case, the layer behaves as an *ideal mass layer*, with response following the Sauerbrey model[8]: resonant frequency decreases in proportion to the areal mass density of the layer, while the quartz crystal resonance remains undamped.

When the film is thicker or more compliant, e.g., a polymer, then the displacement applied by the quartz at the lower film surface can undergo a significant phase shift (and possibly attenuation) in propagating across the layer. As this acoustic phase shift becomes significant, so do the interference effects. When the phase shift reaches $\pi/2$ radians (or an odd multiple thereof), interference becomes constructive, resulting in enhanced absorption of acoustic energy by the film; this condition is called *film resonance*.[9-11] The following characteristics are associated with film resonance: as ϕ increases toward $\pi/2$, the resonant frequency decreases, while resonance damping increases; as ϕ exceeds $\pi/2$, the resonant frequency increases (and can exceed that of the unperturbed crystal), while resonance damping diminishes.

Recently, researchers have noted that these responses can be observed by varying either the thickness[12,13] or temperature[9] of a polymer-coated TSM resonator. Varying either parameter causes the phase shift across the film to vary; if ϕ reaches $\pi/2$ (or an odd multiple) the film resonant response arises. By applying the proper model, film viscoelastic properties can be extracted from these responses.[2]

In this paper, we derive a lumped-element, equivalent-circuit model that approximates the electrical characteristics of the TSM resonator with a *viscoelastic* film in the vicinity of resonance. Any material can be generalized as being viscoelastic where both elastic energy storage and viscous power dissipation are present.[14] The film is represented by a parallel "tank" circuit consisting of a resistor, a capacitor, and an inductor. These elements are explicitly related to the film's mechanical properties. Since the quartz crystal is considered one resonator and the viscoelastic layer another, the result is the representation of the resonator/film combination as two *coupled resonators*.[15,16] The composite response depends on the interaction of these two resonant systems. The simple equivalent-circuit representation elucidates this interaction more clearly than the more complicated

transmission-line model, leading to a simple graphical interpretation for the response. It also leads to a prediction of a double-peaked admittance response under certain circumstances.

THEORY

Model for TSM resonator with a surface load. The complex electrical input impedance for the quartz resonator described by the model in Fig. 3 is:[10]

$$Z = \frac{1}{j\omega C_0}\left[1 - \frac{K^2}{\phi_q}\frac{2\tan(\phi_q/2) - j\zeta}{1 - j\zeta\cot(\phi_q)}\right] \tag{1}$$

where $\omega = 2\pi f$, f is the excitation frequency; C_0 is the resonator static capacitance; K^2 is the quartz electromechanical coupling coefficient; ϕ_q is the complex acoustic wave phase shift across the quartz; $\zeta = Z_L/Z_q$, where Z_L is the load surface mechanical impedance and $Z_q = (\rho_q\mu_q)^{1/2}$ is the quartz characteristic impedance, with ρ_q and μ_q are the quartz density and shear stiffness, respectively; and $j = (-1)^{1/2}$.

The electrical impedance in Eq. 1 can be represented by a static capacitance, C_0, in parallel with a motional impedance, Z_m, arising from piezoelectrically-induced motion: $Z = (j\omega C_0 + 1/Z_m)^{-1}$. Rearranging Eq. 1 gives the motional impedance term:[10]

$$Z_m = \frac{1}{j\omega C_0}\left\{\frac{1 - j\zeta\cot(\phi_q)}{\frac{K^2}{\phi_q}\left[2\tan\left(\frac{\phi_q}{2}\right) - j\zeta\right]} - 1\right\} \tag{2}$$

which can be written as:[10]

$$Z_m = \frac{1}{j\omega C_0}\left[\frac{\phi_q}{2K^2\tan(\phi_q/2)} - 1\right] + \frac{\phi_q \zeta}{4K^2\omega C_0}\left[1 - \frac{j\zeta}{2\tan(\phi_q/2)}\right]^{-1} \qquad (3)$$
$$= Z_1 + Z_2$$

where Z_1 describes the motional impedance for the unperturbed resonator (i.e., without a film), and Z_2 the added motional impedance due to the surface load. Fig. 4a shows the equivalent-circuit representation for the motional impedance contributions in parallel with C_0.

Unperturbed resonator. From Eq. 3, the motional impedance associated with an unperturbed resonator is:

$$Z_1 = \frac{1}{j\omega C_0}\left[\frac{\phi_q}{2K^2\tan(\phi_q/2)} - 1\right] \qquad (4)$$

Near resonance, when $\mathrm{Re}(\phi_q) \cong N\pi$, where N is the *resonator* harmonic number (odd integer), the following approximation can be used for the tangent function:[17]

$$\tan\left(\frac{\phi_q}{2}\right) \cong \frac{4\phi_q}{(N\pi)^2 - \phi_q^2} . \qquad (5)$$

Substituting Eq. 5 into Eq. 4 yields:

$$Z_1 \cong \frac{1}{j\omega C_0}\left[\frac{(N\pi)^2 - \phi_q^2}{8K^2} - 1\right] . \qquad (6)$$

The phase shift across the quartz is the complex quantity $\phi_q = \omega h_q(\rho_q/\mu_q)^{1/2}$, where h_q is the quartz thickness. To account for losses in the quartz, μ_q is represented by the complex quantity: $\mu_q = \mu_{qo} + j\omega\eta_q$, where μ_{qo} is the shear stiffness and η_q is the effective quartz viscosity.[1] Using these quantities in Eq. 6 gives:

$$Z_1 \cong \left(\frac{\omega^2 h_q^2 \rho_q \eta_q}{8K^2 C_0 |\mu_q|^2}\right) + j\omega\left(\frac{h_q^2 \rho_q \mu_{qo}}{8K^2 C_0 |\mu_q|^2}\right) + \frac{1}{j\omega}\left[\frac{(N\pi)^2 - 8K^2}{8K^2 C_0}\right] . \quad (7)$$

A series-connected resistor, R_1, inductor, L_1, and capacitor, C_1, has the impedance:

$$Z_1 = R_1 + j\omega L_1 + \frac{1}{j\omega C_1} \quad (8)$$

which has the same frequency dependence as Eq. 7 assuming we evaluate the first term of Eq. 7 at $\omega = \omega_s$, where $\omega_s = 2\pi f_s$ and f_s is the series resonance frequency. This equivalence is appropriate since Eq. 7 follows from an approximation valid only near crystal resonance. Fig. 4b shows the series LCR elements that approximate the impedance of the unperturbed resonator in the vicinity of quartz resonance.

Comparison between Eqs. 7 and 8 allows identification of the unperturbed circuit element values. Assuming that quartz losses are small, $\omega\eta_q \ll \mu_{qo}$, so that $|\mu_q| \cong \mu_{qo}$, and letting $\omega = \omega_S$ so that $\omega/\omega_S \cong 1$, gives:[17]

$$C_1 = \frac{8K^2 C_0}{(N\pi)^2 - 8K^2} \quad (9a)$$

$$L_1 = \frac{h_q^2 \rho_q}{8K^2 C_0 \mu_{qo}} = \frac{1}{\omega_s^2 C_1} \quad (9b)$$

$$R_1 = \frac{\omega_s^2 h_q^2 \rho_q \eta_q}{8K^2 C_0 \mu_{qo}^2} = \frac{\eta_q}{C_1 \mu_{qo}} \quad (9c)$$

We have used the fact that series resonance occurs when the reactive (imaginary) part of the impedance in Eq. 8 is zero, i.e., when

$$\omega_s^2 = \frac{1}{L_1 C_1} = \frac{\mu_{qo}\left[(N\pi)^2 - 8K^2\right]}{h_q^2 \rho_q} \quad . \tag{10}$$

Contribution from a viscoelastic film. From Eq. 3, the motional impedance contributed by a surface load on the resonator is given by:[10]

$$Z_2 = \frac{\phi_q \zeta}{4K^2 \omega C_0}\left[1 - \frac{j\zeta}{2\tan\left(\phi_q/2\right)}\right]^{-1} \quad . \tag{11}$$

Using the approximation for tan (ϕ_q/2) given by Eq. 5 and noting that $\phi_q \cong N\pi$ near a quartz resonance allows Eq. 11 to be approximated near resonance as:

$$Z_2 \cong \left\{\frac{4K^2 \omega C_o}{N\pi\zeta} + j\frac{\omega K^2 C_0}{2}\left[1 - \left(\frac{\omega_s}{\omega}\right)^2\right]\right\}^{-1} \quad . \tag{12}$$

Since we are interested in the effect of the load on the quartz resonance, we can take $\omega \cong \omega_s$ (the same degree of approximation used in obtaining Eqs. 9), eliminating the second term in Eq. 12, producing:[18]

$$Z_2 \cong \frac{N\pi\zeta}{4K^2 \omega_s C_0} = \frac{N\pi}{4K^2 \omega_s C_0}\left(\frac{Z_L}{Z_q}\right) \quad . \tag{13}$$

An earlier study verified that Eq. 13 is an adequate representation of Eq. 11 for the impedance due to a surface load.[19]

Film Displacement Profile. The surface mechanical impedance, Z_L, of a viscoelastic film is found by first determining the shear displacement generated in the film by the oscillating resonator surface and then calculating the shear stress required to generate this motion. The mechanical impedance

is the ratio of this shear stress to the particle velocity at the resonator/film interface.[20]

The oscillating resonator surface generates a shear displacement profile, $u_x(y)$, across the film (Fig. 2) determined by the equation of motion:[17]

$$G\frac{\partial^2 u_x}{\partial y^2} = \rho \ddot{u}_x \tag{14}$$

where G and ρ are the film's shear modulus and density, respectively. For a viscoelastic film undergoing sinusoidal deformation, the shear modulus, G, is represented by a complex quantity:[14] $G = G' + jG''$. The real part, G', represents the component of stress in-phase with strain, giving rise to energy storage, and is thus called the "storage modulus." The imaginary part, G'', represents the component of stress $\pi/2$ radians out-of-phase with strain, giving rise to power dissipation, and is thus called the "loss modulus."

The solution to Eq. 14 is a superposition of counter-propagating shear waves, one propagating away from the resonator/film interface and one reflected by the film/air boundary:

$$u_x(y,t) = \left(c_1 e^{-\gamma y} + c_2 e^{\gamma y}\right) e^{j\omega t} \tag{15}$$

where c_1 and c_2 are constants and γ is the shear-wave propagation factor (u_x is actually the real part of Eq. 15); γ is determined by substituting Eq. 15 into Eq. 14, yielding:

$$\gamma = j\omega\sqrt{\frac{\rho}{G}} \tag{16}$$

Since G is complex, γ is also, meaning the acoustic wave experiences both a phase delay and attenuation while traversing the film.

The constants c_1 and c_2 in Eq. 15 are determined by applying two boundary conditions that arise at the upper and lower film surfaces (see Fig. 2): (1) continuity of particle displacement at the

resonator/film interface gives $u_x(0^-) = u_x(0^+)$, and (2) the stress-free boundary at the film/air interface gives $\partial u_x/\partial y|_{y=h} = 0$, where h is the film thickness. Applying these two conditions, solving for c_1 and c_2, and inserting these into Eq. 15 gives:

$$u_x(y,t) = u_{xo}\left\{\frac{\cosh\left[\gamma(h-y)\right]}{\cosh(\gamma h)}\right\}e^{j\omega t} \tag{17}$$

where u_{xo} is the displacement at the resonator surface (u_x is the real part of Eq. 17).

Surface mechanical impedance due to film. The mechanical impedance at the resonator/film interface is given by:[20]

$$Z_L = -\left.\frac{T_{xy}}{v_x}\right|_{y=0} = -\left.\frac{G}{j\omega u_x}\frac{\partial u_x}{\partial y}\right|_{y=0} \tag{18}$$

where T_{xy} is the shear stress in the x-direction on a y-normal plane and v_x is the particle velocity in the x-direction. Substituting Eq. 17 into Eq. 18 gives the surface mechanical impedance due to a viscoelastic film:[9]

$$Z_L = \sqrt{\rho G}\tanh(\gamma h) \quad . \tag{19}$$

Lumped-element model near film resonance. Substituting Eq. 19 into Eq. 13 gives an expression for the motional impedance contributed by a finite viscoelastic layer:[9]

$$Z_2 = A\sqrt{\rho G}\tanh(\gamma h) \tag{20}$$

where

$$A = \frac{N\pi}{4K^2\omega_s C_0 Z_q} \tag{21}$$

Noting that $\tanh(jx) \equiv j\tan(x)$, and invoking Eq. 5 to approximate the tangent function, yields:

$$\tanh(\gamma h) \cong \frac{8\gamma h}{(N'\pi)^2 + (2\gamma h)^2} \tag{22}$$

where N' is the *film* harmonic number (odd integer). Eq. 22 is valid near film resonance, i.e., when $\mathrm{Im}(\gamma h) \cong N'\pi/2$. Substituting Eq. 22 into Eq. 20, gives the following approximation for the motional electrical impedance contributed by a viscoelastic film:

$$Z_2 \cong \left[\frac{\omega h G''}{2A|G|^2} + j\omega\left(\frac{hG'}{2A|G|^2}\right) + \frac{1}{j\omega}\left(\frac{(N'\pi)^2}{8Ah\rho}\right)\right]^{-1} . \tag{23}$$

A parallel combination of a resistor R_2, capacitor C_2, and inductor L_2, has an impedance given by:

$$Z_2 = \left[\frac{1}{R_2} + j\omega C_2 + \frac{1}{j\omega L_2}\right]^{-1} \tag{24}$$

which has the same frequency dependence as Eq. 23 if we evaluate the first term of Eq. 23 at $\omega = \omega_S$. This parallel combination of elements thus can be used to represent the frequency dependence of the motional impedance contributed by the viscoelastic film. Comparison between Eqs. 23 and 24 indicates the appropriate values for R_2, C_2, and L_2:

$$R_2 = \frac{2A|G|^2}{\omega h G''} = \frac{N\pi}{2K^2\omega_s^2 C_0 Z_q}\frac{|G|^2}{hG''} \tag{25a}$$

$$C_2 = \frac{hG'}{2A|G|^2} = \frac{2K^2\omega_s C_0 Z_q}{N\pi}\frac{hG'}{|G|^2} \tag{25b}$$

$$L_2 = \frac{8Ah\rho}{(N'\pi)^2} = \frac{2N}{(N')^2\pi K^2\omega_s C_0 Z_q}h\rho \tag{25c}$$

Fig. 4b shows the complete equivalent-circuit model for the resonator loaded with a viscoelastic film, valid near film resonance. (The change in static capacitance, C_0, due to the film has not been considered; this effect should be significant only away from film resonance when the capacitive branch of the equivalent circuit dominates.) As described above, the parallel LCR elements arise from the viscoelastic film. R_2 represents *viscous dissipation* in the film; losses vary as $1/R_2$, proportional to $hG''/|G|^2$. (For a lossless film, G'' is zero, $R_2 \rightarrow \infty$ and R_2 disappears from the model.) C_2 represents *elastic energy storage* in the film and is proportional to $hG'/|G|^2$. L_2 represents *kinetic energy storage* in the film and is proportional to $h\rho$.

The electrical impedance contributed by an "ideal mass layer"—a layer with negligible acoustic attenuation and phase shift across the layer—is:[18,21]

$$Z_{\text{iml}} = jA\omega h\rho \ . \tag{26}$$

The ideal mass layer is represented in an equivalent-circuit model by a single element—an inductance $L_2^{\text{iml}} = Ah\rho$.[18,21] This inductance does not change the impedance magnitude but causes a frequency shift given by the Sauerbrey equation.[8] We note that L_2 arising from the film resonance model (Eq. 25c) is $[8/(N'\pi)^2]L_2^{\text{iml}} \cong 0.81\ L_2^{\text{iml}}$ (for $N' = 1$). This leads to a discrepancy between the Sauerbrey model and the new lumped-element model when $\phi \ll \pi/2$.

Film resonance occurs when the reactive component of the impedance in Eq. 24 is zero. This occurs at an angular frequency:

$$\omega_f = \frac{1}{\sqrt{L_2 C_2}} = \frac{N'\pi|G|}{2h\sqrt{\rho G'}} \quad . \tag{27}$$

At this resonant frequency, the film contributes only a real impedance, R_2, to the motional branch of the equivalent-circuit; this leads to maximum damping of the crystal resonance. Using Eq. 27 in Eq. 23, then dividing by the ideal mass layer contribution (Eq. 26), gives a new expression for the motional impedance contributed by a viscoelastic film near resonance:

$$\frac{Z_2}{Z_{\text{iml}}} = -\frac{8}{(N'\pi)^2} \frac{j(\omega_f/\omega)^2}{(G''/G') + j\left[1-(\omega_f/\omega)^2\right]} \quad . \tag{28}$$

We note that this response depends only on the excitation frequency relative to the film resonant frequency (ω/ω_f) and the film loss tangent (G''/G').

DISCUSSION

Fig. 5 shows a plot of the magnitude and phase of Z_2/Z_{iml} vs. ω/ω_f, calculated from Eq. 28, for $N' = 1$ and several values of G''/G'. For an acoustically thin film, $\omega/\omega_f \ll 1$, the lumped-element model predicts $|Z_2/Z_{\text{iml}}| \cong 0.81$, as indicated previously, for all values of film loss tangent. While we would not expect the lumped-element model to give good predictions far from film resonance, this is a reasonable approximation. At film resonance, $\omega/\omega_f = 1$, the impedance magnitude varies significantly from that of an ideal mass layer and is strongly dependent on the loss tangent. For low-loss films ($G''/G' \ll 1$), the impedance is enhanced compared to the ideal mass layer, while for very lossy films ($G''/G' \gg 1$), the opposite occurs. For $\omega/\omega_f \gg 1$, the impedance magnitude again converges for all loss tangent values, only this time to zero since the excitation frequency is now far from the first film resonance ($N' = 1$). In the lower plots of Fig. 5, the impedance phase angle is shown to lag that of the ideal mass layer. The phase angle also depends strongly on the film loss tangent, except at film resonance where it lags the ideal mass case by exactly $\pi/2$. Note that for low-

loss films, the phase lag approaches π when $\omega/\omega_f \gg 1$.

Model comparisons. Fig. 6 shows a comparison between the transmission-line, lumped-element, and Sauerbrey models. The normalized impedance magnitude and phase are considered for a low-loss film ($G''/G' = 0.2$) and a high-loss film ($G''/G' = 4$). Near film resonance, the lump-element model is a very good approximation for the general transmission-line model when the film is low loss. This is seen in both the magnitude and phase plots of Fig. 6. However, for the high-loss film, the lumped-element model is much less accurate. This deviation arises because the approximation given in Eq. 22, upon which the model is based, utilizes the entire argument γh, while film resonance only depends on the phase shift ϕ, which is the imaginary component of γh. With γ the complex quantity defined in Eq. 16, the phase shift across the viscoelastic film is:[22]

$$\phi = \mathrm{Im}(\gamma h) = \frac{\omega h}{|G|}\sqrt{\frac{\rho(|G| + G')}{2}} \quad . \tag{29}$$

Film resonance occurs when $\phi = N'\pi/2$; using this in Eq. 29 gives an expression for the film resonance as predicted by the transmission-line model:[22]

$$(\omega_f)_{TLM} = \frac{N'\pi|G|}{2h}\sqrt{\frac{2}{\rho(|G| + G')}} \quad . \tag{30}$$

This expression is very similar to that for the lumped-element model, Eq. 27. A ratio of the film resonant frequencies predicted by the two models shows a dependence only on the film loss tangent:[22]

$$\frac{(\omega_f)_{LEM}}{(\omega_f)_{TLM}} = \left[\frac{1 + \sqrt{1 + (G''/G')^2}}{2}\right]^{1/2} \quad . \tag{31}$$

For the two films considered in Fig. 6, the deviations in resonant frequency between the models is 0.5% and 60% for the low-loss and high-loss films, respectively.

Away from film resonance, the lumped-element equivalent circuit model is not always a good approximation to the transmission-line model (Fig. 6). For the acoustically thin films, $\omega/\omega_f \leq 0.3$, the lumped-element model impedance magnitude is 0.81 that of the ideal mass layer, as discussed previously. In this acoustic region, though, the Sauerbrey model is a valid approximation. Also, for excitation frequencies much greater than the film resonance frequency ($\omega/\omega_f \gg 1$), large model deviations occur. Some of these differences are due to the film harmonic resonances predicted by the general transmission-line theory that are not expressed adequately for the lumped-element model in Eq. 28 with $N' = 1$. Better agreement for one of the higher harmonic resonances can be achieved by appropriate choice of N' (odd integer); however, model deviations would then occur at all other film resonances.

Graphical interpretation of resonant response. The response of the TSM resonator plus viscoelastic film depends on the linear combination of the resonator and film motional impedances. The left side of Fig. 7 shows the motional impedance contributions from the quartz resonator $|Z_1|$, the viscoelastic film $|Z_2|$, and the resonator-film composite $|Z_1 + Z_2|$ with progressive deposition of a viscoelastic film. The right side shows the admittance magnitude responses $|Y| = |Z_1 + Z_2|^{-1}$ that result from the composite. The impedance magnitude of the unperturbed resonator $|Z_1|$, represented by the series elements L_1, R_1, and C_1 (Eq. 8), is *minimum* at resonance and increases linearly away from resonance. The angular resonant frequency of the unperturbed resonator is $\omega_s = (L_1C_1)^{-1/2}$. In the graphical example of Fig. 7, the series resonant frequency, f_S, is fixed at 5 MHz. The impedance magnitude contributed by the film, $|Z_2|$, represented by the parallel combination of L_2, C_2, and R_2 (Eq. 24), is *maximum* at film resonance and varies with a Lorentzian frequency dependence (Eq. 28) around ω_f.

Because the unperturbed resonator elements (series L_1, R_1, C_1) and the film elements (parallel L_2, R_2, C_2) are connected in series, the total motional impedance is the sum of both impedance contributions. The solid curve in Fig. 7 is the magnitude of the sum of the impedances $|Z_1 + Z_2|$. Due to the limited bandwidth of the resonator, the effect of the film on resonator response does not become pronounced until there is significant overlap between the film and resonator resonances, i.e.,

until ω_f approaches ω_s.

Since the film resonant frequency is dependent upon film thickness h, modulus G, and density ρ (Eq. 27), film resonance can be made to approach, and pass through, the quartz resonant frequency by varying any of these properties. For the example in Fig. 7, the film resonant frequency decreases with increasing film thickness. When $\omega_f > \omega_s$, the composite impedance magnitude $|Z_1 + Z_2|$ exhibits a resonance at a frequency smaller than ω_s (Fig. 7a1). This lower resonance frequency is also reflected in the peak admittance magnitude (b1). As ω_f approaches ω_s, the composite resonant frequency decreases further, and the minimum impedance increases, reflecting increased crystal damping (a2). Additionally, a "shoulder" appears in the $|Z_1 + Z_2|$ curve near ω_f due to the film resonance. The decrease in resonant frequency and increase in resonance damping appear in the overall admittance response (b2). When $\omega_f \cong \omega_s$, the composite impedance magnitude $|Z_1 + Z_2|$ shows two minima, each with relatively high impedance, occurring at frequencies far from ω_s (a3). In the corresponding admittance plot (b3), this resonance interference produces a split, highly damped response. As ω_f decreases below ω_s, the resonant frequency of the composite is greater than ω_s and the damping diminishes (a4, a5). The single resonance peak in the admittance magnitude re-emerges at a frequency higher than ω_s (b4, b5).

The double-peak admittance response (Fig. 7b3) is observed only when the film loss is low, so that the film impedance bandwidth is comparable to the width of the quartz motional impedance at the point of overlap. For lossier films, for which the film impedance peak is very broad, a single admittance peak results. This feature is illustrated in Fig. 8 where the resonator and the film impedance magnitudes (upper) and the composite admittance magnitude (lower) are plotted around film resonance for several arbitrary values of the film loss tangent. For the lowest loss film (small G''/G'), $|Z_2|$ has a narrow resonance peak achieving a large maximum impedance value. Since the film impedance bandwidth is narrower than the resonator impedance magnitude region $|Z_1|$, the composite admittance magnitude shows two well-defined maxima. As the film loss increases (increasing G''/G'), the film impedance magnitude broadens in the region where it overlaps the resonator impedance magnitude, and the admittance double peaks diminish in magnitude and move toward the crystal resonant frequency. Eventually, the admittance peaks merge into a single

maximum at ω_s when the film impedance bandwidth is wider than the resonator impedance overlap region. The double-peak feature is determined solely by the viscoelastic film modulus, both its magnitude and the loss tangent, with transition to a single maximum occurring when $\log_{10}G'' \approx \sqrt{2}$ $(\log_{10}G' - 2)$.[23]

Displacement profiles. The response of a quartz resonator loaded with a viscoelastic film can be related to its dynamic film behavior. Fig. 9 shows shear displacement profiles in the film, calculated from Eq. 17, using the film thicknesses indicated in Fig. 7 and evaluated at the frequencies of peak admittance (7b). These displacements are normalized to constant power dissipation. When the film phase shift is significantly below resonance, the film displacement is in-phase with the driving quartz resonator surface displacement (Fig. 9a). The displacement at the film/air interface is actually much greater than at the resonator surface—overshoot occurs. When ϕ is significantly above resonance (Fig. 9f), the film displacement is predominantly π radians out-of-phase with the driving quartz resonator surface displacement. In the vicinity of film resonance (Fig. 9b-e), there is a rapid phase variation between the upper and lower film surfaces. Additionally, due to the greater power dissipation in the film, the quartz displacement is diminished; this leads to the highly damped admittance responses seen in Fig. 7b2-7b4. Curves c and d in Fig. 9 are calculated at the two admittance peaks indicated in Fig. 7b3. We note the phase reversal of film displacement between these two peaks.

Resonance conditions and modes. We can further understand the dynamic behavior of the quartz resonator plus viscoelastic film by considering the combination as a coupled resonant system. The quartz alone can be considered as having two low-impedance surfaces, since the film mechanical impedance is typically much less than the quartz impedance ($Z_L \ll Z_q$). When a shear wave propagates in this quartz transmission line (Fig. 10a), the low-impedance surfaces give rise to a reflection phase $\phi_R = 0$. Resonance occurs when the round-trip phase shift is a multiple of 2π radians. This gives a resonance condition of:

$$2k_q h_q = 2N\pi \tag{32}$$

where k_q is the shear-wave propagation factor in quartz: $k_q=\omega(\rho_q/\mu_q)^{1/2}$. Because electrical excitation of the quartz resonator can occur only at the odd harmonics, N in Eq. 32 must be an odd integer. The resonance condition of Eq. 32 is satisfied when $h_q = N\lambda_q/2$, where λ_q is the shear acoustic wavelength in quartz; this corresponds to a phase shift $\phi_q = N\pi/2$. Resonance conditions in the quartz lead to a standing wave, shown in quartz Fig. 10a, with antinodes (displacement maxima) at the two surfaces.

On the other hand, the film alone has a high-impedance interface (film/quartz) and a low-impedance interface (film/air). For a shear wave executing a round trip in this film transmission line, the high-impedance surface contributes a reflection phase $\phi_R = \pi$, while the low-impedance surface has $\phi_R = 0$. The resonance condition in the film is then:

$$2\gamma h + \pi = 2N'\pi \,. \tag{33}$$

Again, only the odd harmonics can be excited, so N' must be an odd integer. Eq. 33 is satisfied when $h = (2N' - 1)\lambda/4$, where λ is the shear acoustic wavelength in the film. This corresponds to a film phase shift $\phi = N'\pi/2$. The resonance conditions in the quartz and film are different since the boundary conditions are different. The standing wave in the film consists of a "virtual" node at the quartz/film interface and an antinode at the film/air interface (Fig. 10b).

The quartz resonator and film combination exhibit characteristics of coupled resonant systems: displacement in the resonator/film has both in-phase and out-of-phase modes, with a concurrent *splitting of resonant frequency* into two corresponding branches. While independently the quartz and film each have a distinct resonant frequency, when the two are coupled, two distinct system resonances arise. This splitting is visible in Fig. 7b3 where two admittance peaks are observed. In Fig. 10b for $\phi = (\pi/2)^-$, the upper film displacement is large and in-phase with the driving resonator surface. For $\phi = (\pi/2)^+$, the upper film surface is π radians out-of-phase with the drive surface and the resultant frequency is higher than for the unperturbed quartz resonator.

CONCLUSIONS

A new equivalent-circuit model has been derived that is valid near film resonance and is a

reasonable approximation away from resonance. This model consists of a *series* LCR resonator, representing the quartz impedance near its resonance, and a *parallel* LCR resonator, representing the viscoelastic film impedance near its resonance. Elements corresponding to the film are explicitly related to the film's mechanical properties and represent energy storage and power dissipation.

This new model and the Sauerbrey model both approximate the more detailed transmission-line model in various regimes defined by acoustic phase shift across the viscoelastic layer. The Sauerbrey model works well for acoustically thin films with $\phi < \pi/4$. The viscoelastic layer is then treated as an ideal mass layer, with response dependent only on its areal mass density. The new model works well when $\phi \approx \pi/2$ and the film's losses are relatively low, $G''/G' < 1$. The film resonance characteristics then define the surface load; response depends on both the density and shear modulus of the film. Each model leads to a simplified analysis and interpretation for sensor applications or material characterizations.

The TSM resonator and the viscoelastic film can be considered as coupled resonators.[15,16] Individually, the resonant conditions for the quartz and film are different, due to the non-symmetric boundary conditions imposed at the film-to-quartz interface: looking into the film, the quartz sees a low-impedance interface, while looking into the quartz, the film sees a high-impedance interface. The response of the composite resonator (quartz resonator plus film) depends on the interaction of the individual quartz and film resonances. A simple graphical representation involving the series and parallel impedances illustrates the composite resonator response. While independently the quartz and film each have a distinct resonant frequency, when the two are coupled, two system resonances can arise. These correspond to different displacement profiles in the film that are shifted by a π phase shift.

The gross features predicted by the new equivalent-circuit model, including frequency changes and increased damping near film resonance, have been observed experimentally.[9-13] In fact, even polymer films deposited in aqueous solutions produce the film-resonant responses.[12,13] This may be somewhat surprising, in view of the stress-free boundary assumed at the upper film surface. The film/fluid interaction would seem to be too lossy to give rise to a resonant response. However, calculations show that the liquid impedance can be significantly smaller than that of the film so that acoustic reflection at the film/liquid interface is sufficient for film resonance to

occur. The present model is a reasonable approximation in this case; a more accurate model could be derived that properly accounts for the film/liquid interface.

The fine features predicted by the current model, including the double-peak admittance response when quartz and film resonances coincide, have yet to be conclusively observed. Most likely this is due to the viscoelastic films being too lossy to satisfy the condition required for their emergence. A properly designed experiment, including a low-loss film with the required $\pi/2$ phase shift, may succeed in eliciting this response.

ACKNOWLEDGMENT

Sandia is a multiprogram laboratory operated by Sandia Corporation, a Lockheed Martin Company, for the United States Department of Energy under Contract DE-AC04-94AL85000.

REFERENCES

(1) Reed, C.E.; Kanazawa, K.K.; Kaufman, J.H. *J. Appl. Phys.* **1990**, *68*, 1993-2001.

(2) Bandey, H.L.; Martin, S.J.; Cernosek, R.W.; Hillman, A.R. *Anal. Chem.* **1999**, *71*, 2205-2214.

(3) Behling, C.; Lucklum, R.; Hauptmann, P. *Meas. Sci. Technol.* **1998**, *9*, 1886-1893.

(4) Wolff, O.; Seydel, E.; Johannsmann, D. *Faraday Discuss.* **1997**, *107*, 91-104.

(5) Calvo, E.J.; Etchenique, R.; Bartlett, P.N.; Singhal, K.; Santamaria, C.; *Faraday Discuss.* **1997**, *107*, 141-157.

(6) Hillman, A.R.; Bandey, H.L.; Gonsalves, M.; Bruckenstein, S.; Pater, E. *Annali Di Chimica* **1997**, *87*, 177-186.

(7) Mason, W.P. *Physical Acoustics*; Academic Press: New York, 1965. Vol. II, Part A.

(8) Sauerbrey, G. *Z. Phys.* **1959**, *155*, 206-222.

(9) Martin, S.J.; Frye, G.C. *Ultrason. Symp.* **1991**, 393-398.

(10) Lucklum, R.; Behling, C.; Cernosek, R.W.; Martin, S.J. *J. Phys. D: Appl. Phys.* **1997**, *30*, 346-356.

(11) Martin, S.J; Frye, G.C.; Senturia, S.D. *Anal. Chem.*, **1994**, *66*, 2201-2219.

(12) Hillman, A.R.; Brown, M.J.; Martin, S.J. *J. Am. Chem. Soc.* **1998**, *120*, 12968-12969.

(13) Saraswathi, R.; Hillman, A.R.; Martin, S.J. *J. Electroanal. Chem.* **1999**, *460*, 267-272.

(14) Ferry, J. D. *Viscoelastic Properties of Polymers*; Wiley: New York, 1980. Ch. 17. 3rd ed.

(15) Benes, E. *J. Appl. Phys.* **1984**, *56*, 608-626.

(16) Mecea, V.M. *Sensors and Actuators A*, **1994**, *40*, 1-27.

(17) Rosenbaum, J. F. *Bulk Acoustic Wave Theory and Devices*; Artech House: Boston, 1988.

(18) Martin, S.J.; Frye, G.C.; Ricco, A.J.; Senturia, S.D. *Anal. Chem.* **1993**, *65*, 2910-2922.

(19) Cernosek, R.W.; Martin, S.J.; Hillman, A.R.; Bandey, H.L. *IEEE Trans. Ultrason., Ferroelectr. Freq. Cont.* **1998**, *45*, 1399-1407.

(20) Auld, B. A. *Acoustic Fields and Waves in Solids*; Wiley: New York, 1973. Ch. 7. Vol. I.

(21) Martin, S.J.; Granstaff, V.E.; Frye, G.C. *Anal. Chem.*, **1991**, *63*, 2272-2281.

(22) Cernosek, R.W.; Martin, S.J.; Bandey H.L; Hillman A.R. *Eurosensors XIII Conf.*, Sept. 12-15, 1999, The Hague, The Netherlands.

(23) Bandey, H.L.; Cernosek, R.W.; Martin, S.J. *196th Meeting of the Electrochem. Soc.*, Oct. 17-22,

1999, Honolulu, HI.

FIGURE CAPTIONS

Fig. 1 Thickness shear mode resonator: (a) top and side views, (b) shear displacement.

Fig. 2 Cross-sectional view of a quartz resonator with a viscoelastic film coating the upper surface. The film thickness is exaggerated relative to that of the quartz. The potential, V, creates the shear deformation in the crystal.

Fig. 3 Transmission-line model for a quartz resonator with a viscoelastic film coating the upper surface; n and X are defined in Ref. 10.

Fig. 4 Equivalent-circuit models for a quartz resonator with a viscoelastic film: (a) general equivalent-circuit representation, and (b) lumped-element representation for the quartz and the film, valid near a film resonance.

Fig. 5 Impedance response, normalized to that of an ideal mass layer, vs. normalized excitation frequency for several values of the film loss tangent G''/G' and $N' = 1$.

Fig. 6 Normalized impedance response vs. normalized excitation frequency, calculated from the transmission-line, lumped-element, and Sauerbrey models for low- and high-loss films.

Fig. 7 Effect of varying film thickness on (a) impedance magnitude for a quartz resonator $|Z_1|$, a viscoelastic film $|Z_2|$, and the composite $|Z_1 + Z_2|$; (b) resulting admittance response. The film parameters are $\rho = 1$ g cm^{-3}, $G' = 10^8$ dyne cm^{-2}, and $G''/G' = 0.1$.

Fig. 8 The contributing impedance magnitudes (upper) and composite admittance magnitude (lower) for a 5 MHz resonator operating near film resonance. The transition from two resonant peaks to one occurs as the film loss tangent (G''/G') increases.

Fig. 9 Shear displacement profiles in the quartz resonator and the viscoelastic film (normalized thicknesses) calculated for the film thicknesses of Fig. 7 at the admittance peaks.

Fig. 10 Modes of shear vibration at the fundamental resonance: (a) in quartz, and (b) in the film. In the composite (coupled resonators), frequency splitting occurs.

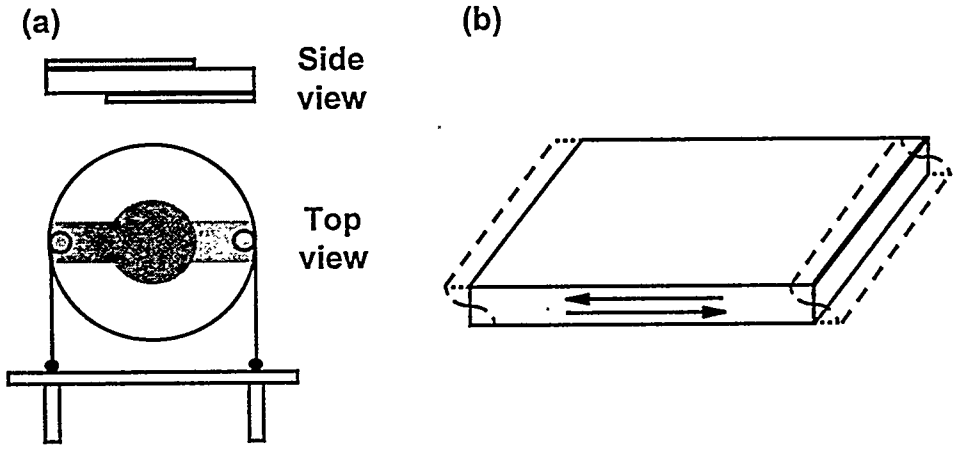

Fig. 1 Thickness shear mode resonator: (a) top and side views, (b) shear displacement.

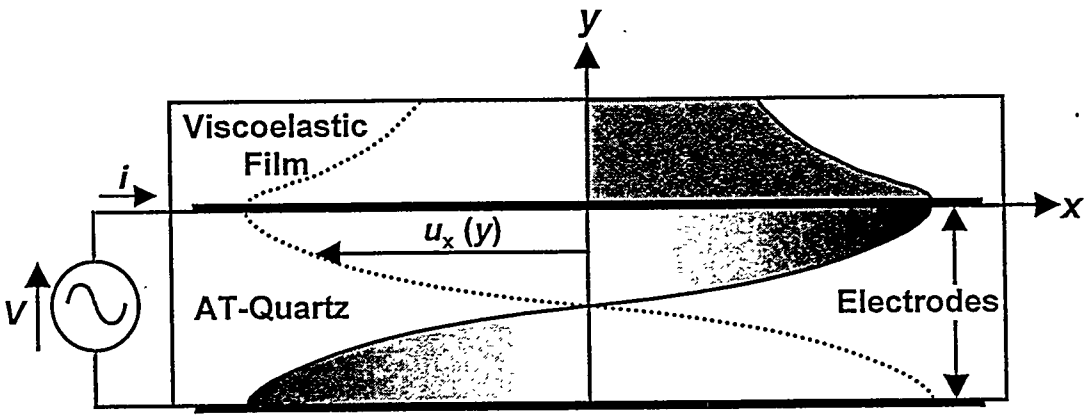

Fig. 2 Cross-sectional view of a quartz resonator with a viscoelastic film coating the upper surface. The film thickness is exaggerated relative to that of the quartz. The potential, V, creates the shear deformation in the crystal.

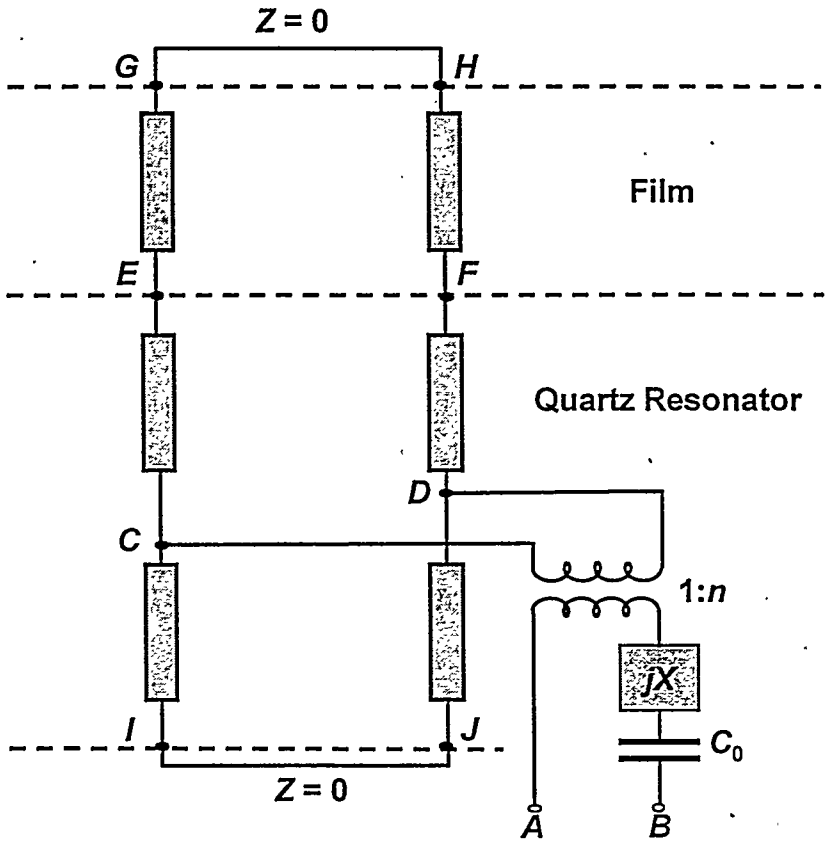

Fig. 3 Transmission-line model for a quartz resonator with a viscoelastic film coating the upper surface; n and X are defined in Ref. 15.

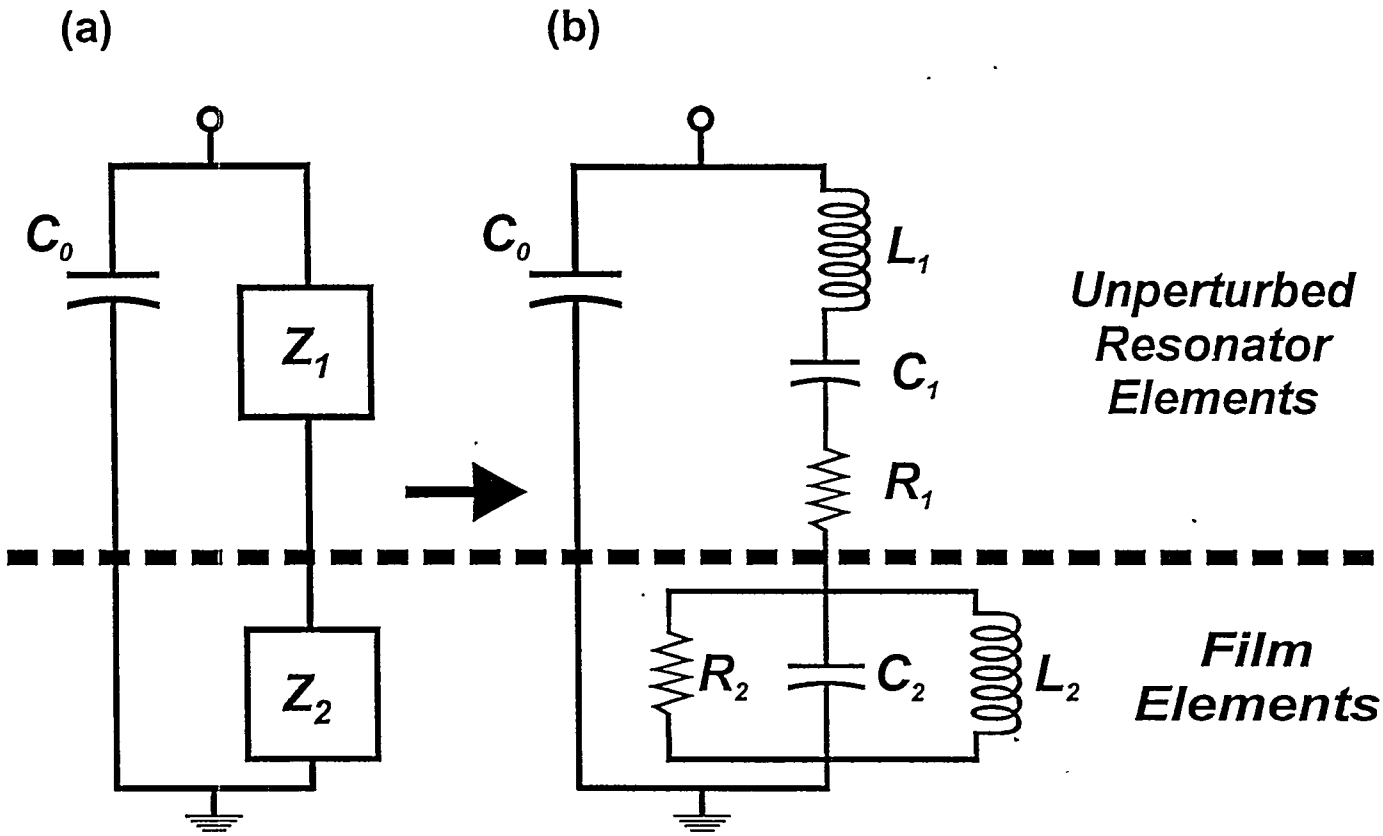

Fig. 4 Equivalent-circuit models for a quartz resonator with a viscoelastic film: (a) general equivalent-circuit representation, and (b) lumped-element representation for the quartz and the film, valid near a film resonance.

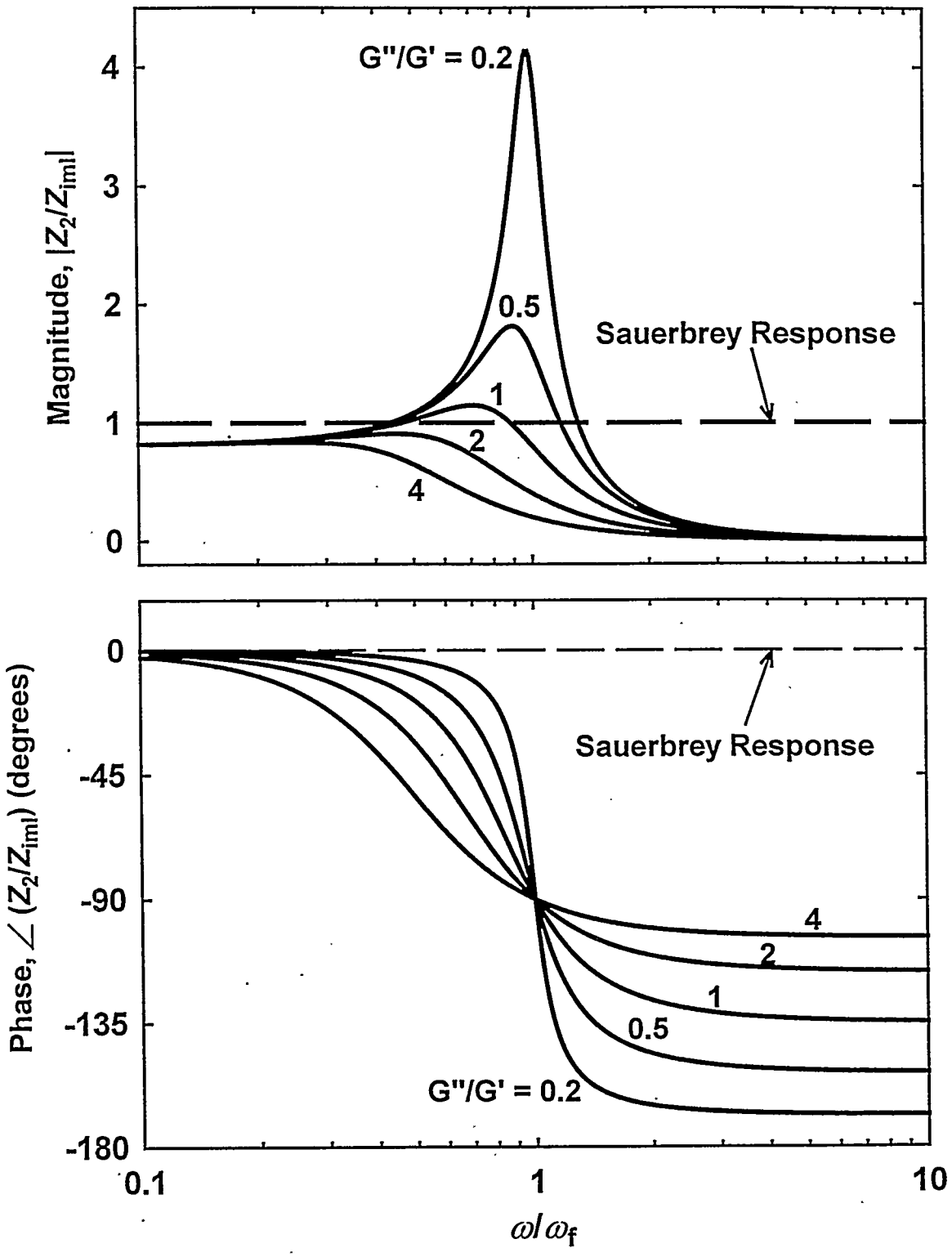

Fig. 5 Impedance response, normalized to that of an ideal mass layer, vs. normalized excitation frequency for several values of the film loss tangent G''/G' and $N' = 1$.

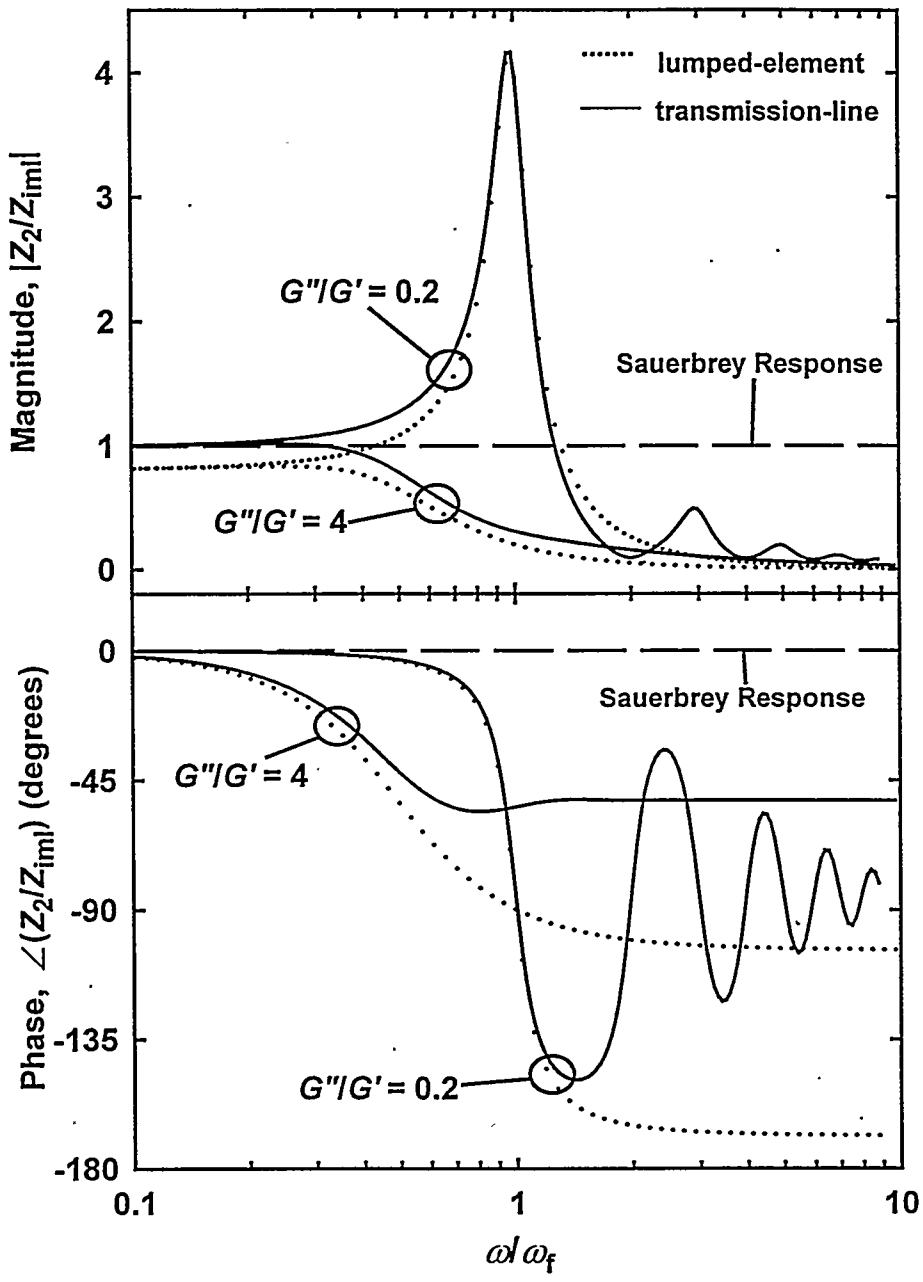

Fig. 6 Normalized impedance response vs. normalized excitation frequency, calculated from the transmission-line, lumped-element, and Sauerbrey models for low- and high-loss films.

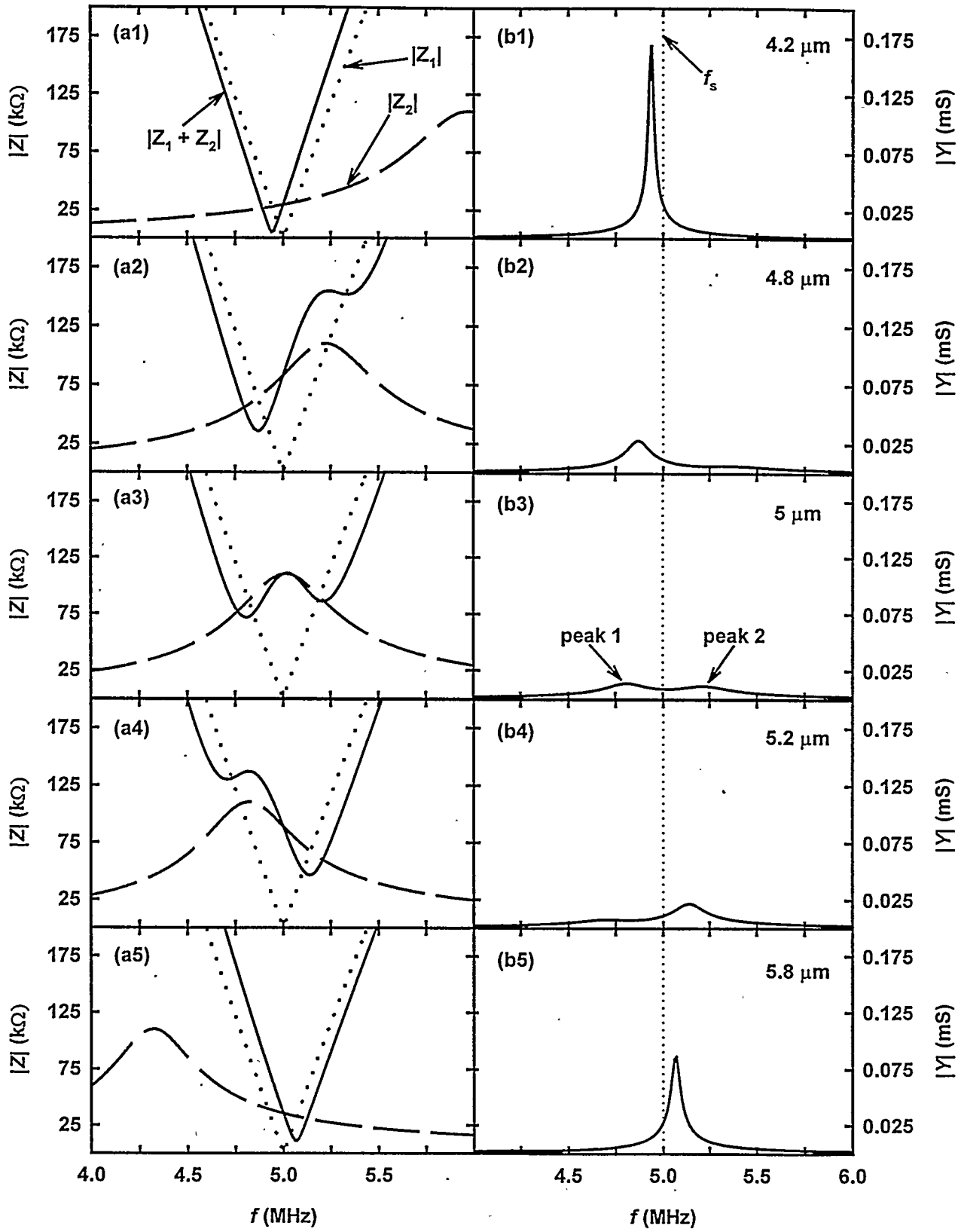

Fig. 7 Effect of varying film thickness on (a) impedance magnitude for a quartz resonator $|Z_1|$, a viscoelastic film $|Z_2|$, and the composite $|Z_1 + Z_2|$; (b) resulting admittance response. The film parameters are $\rho = 1$ g cm^{-3}, $G' = 10^8$ dyne cm^{-2}, and $G''/G' = 0.1$.

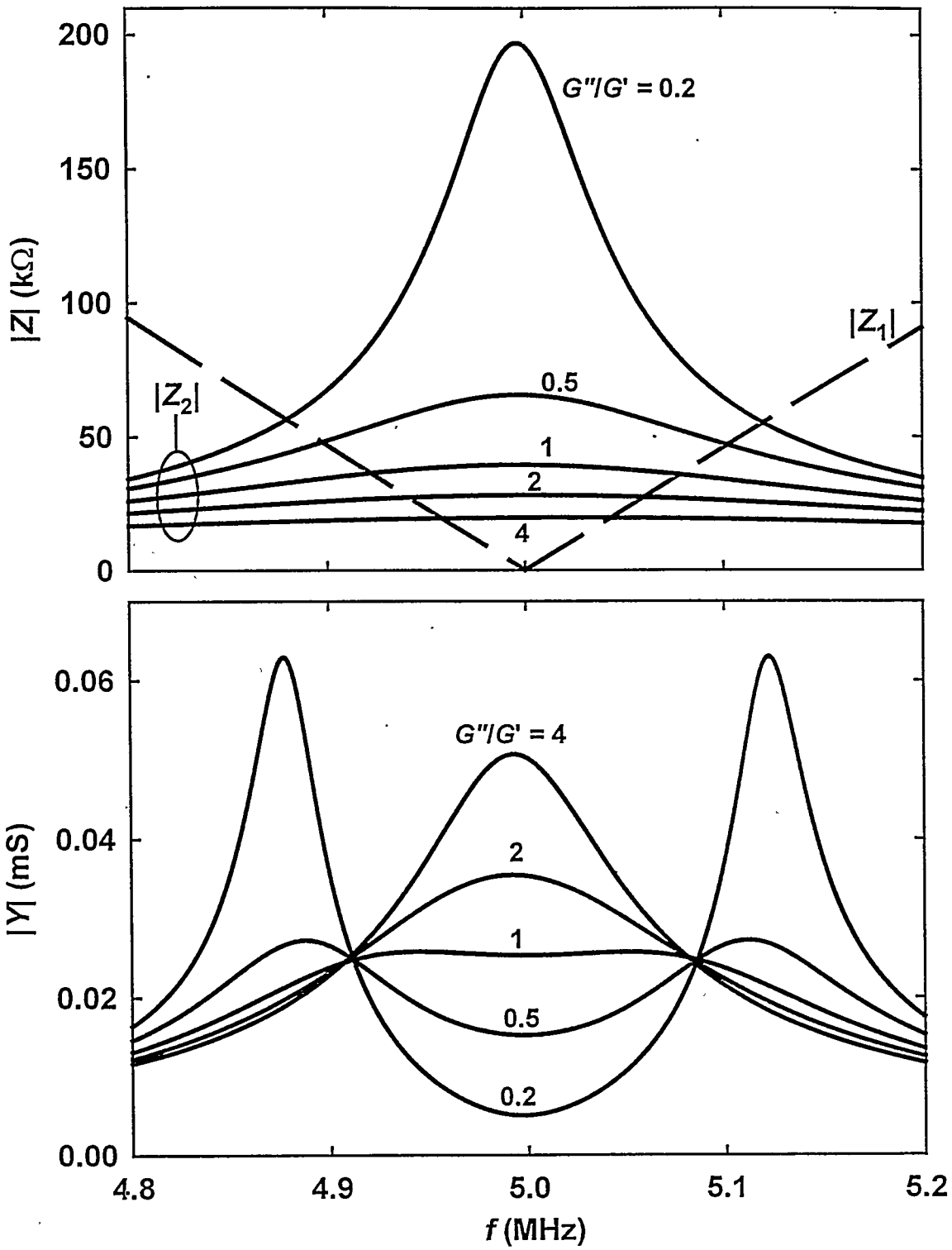

Fig. 8 The contributing impedance magnitudes (upper) and composite admittance magnitude (lower) for a 5 MHz resonator operating near film resonance. The transition from two resonant peaks to one occurs as the film loss tangent (G''/G') increases.

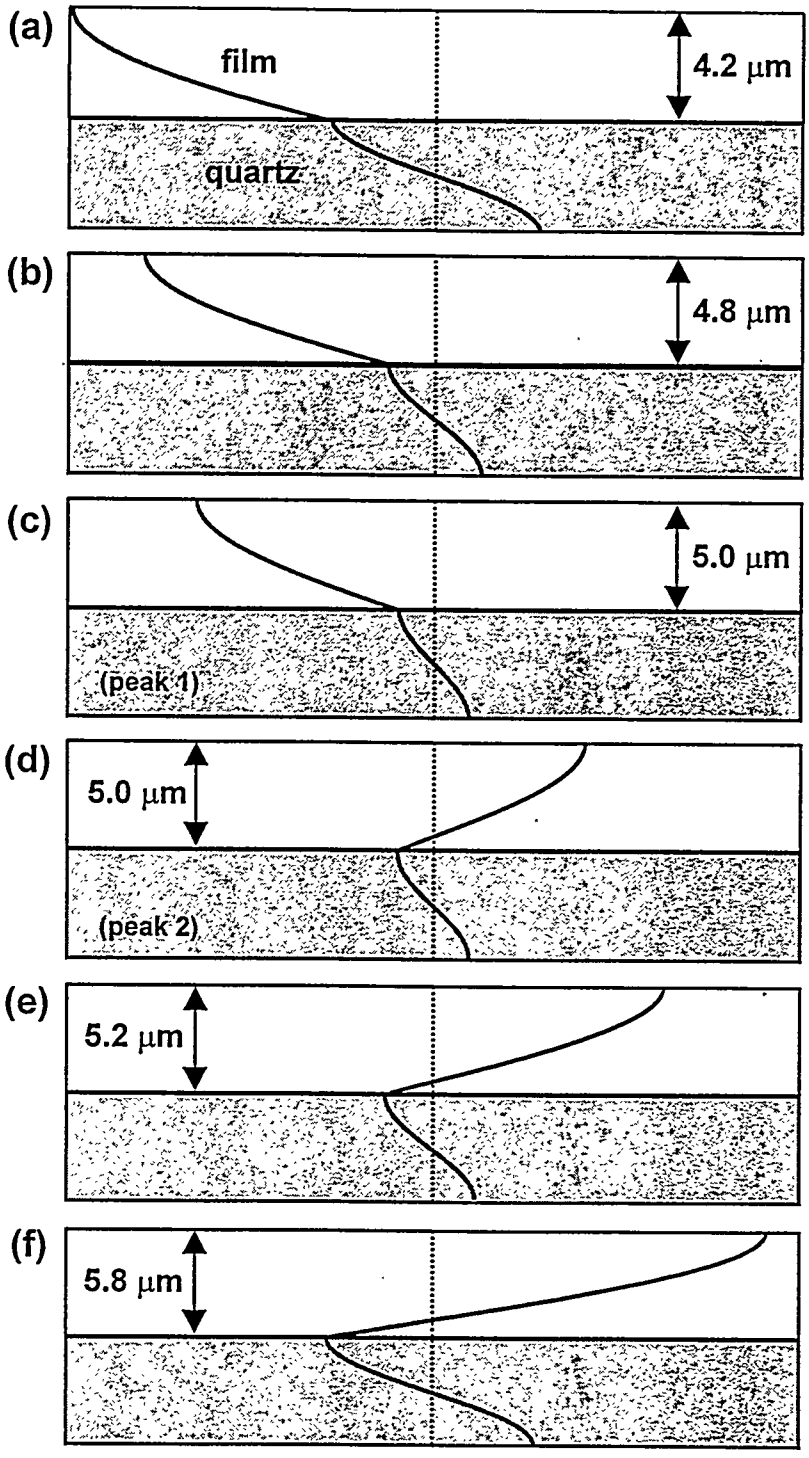

Fig. 9 Shear displacement profiles in the quartz resonator and the viscoelastic film (normalized thicknesses) calculated for the film thicknesses of Fig. 7 at the admittance peaks.

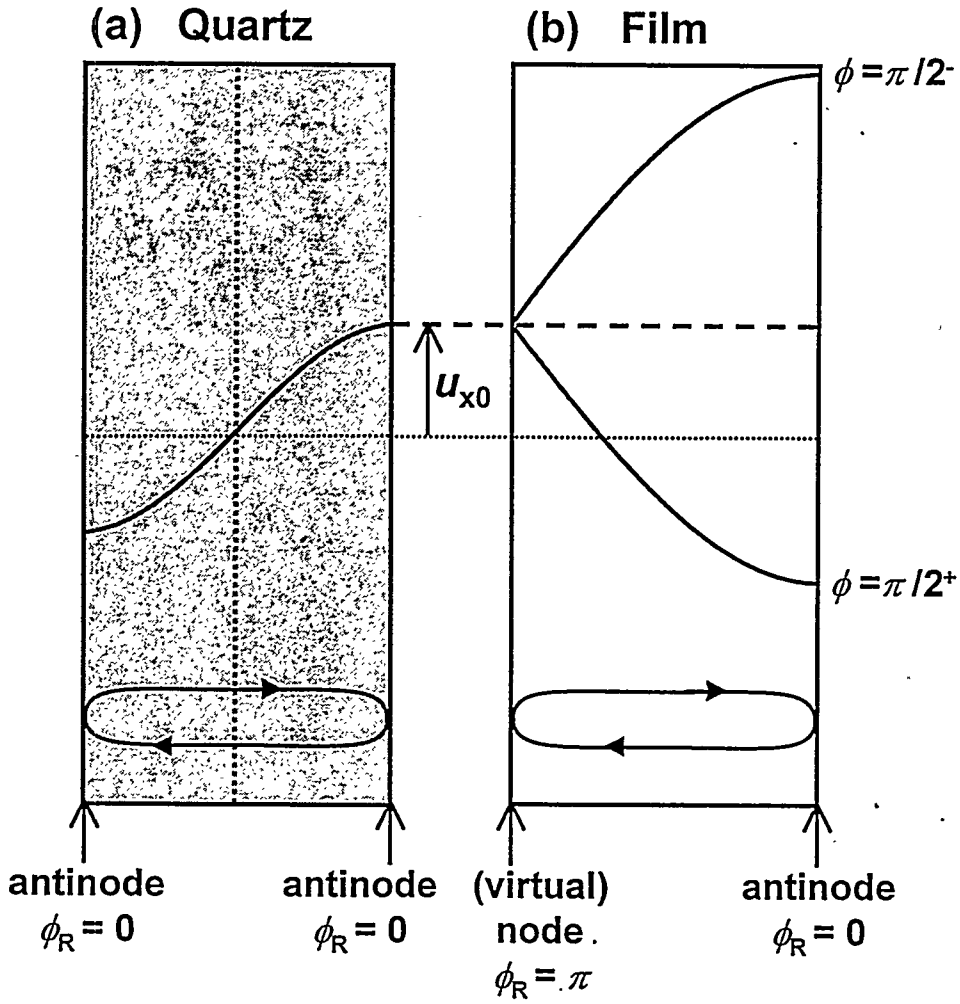

Fig. 10 Modes of shear vibration at the fundamental resonance: (a) in quartz, and (b) in the film. In the composite (coupled resonators), frequency splitting occurs.